Journal of Hazardous Materials 191 (2011) 32–40

Contents lists available at ScienceDirect

Journal of Hazardous Materials

journal homepage: www.elsevier.com/locate/jhazmat

Molecular mechanism of hippocampal apoptosis of mice following exposure to titanium dioxide nanoparticles

Renping Hu[a,1], Lei Zheng[a,1], Ting Zhang[b,c,1], Guodong Gao[a,1], Yaling Cui[a], Zhe Cheng[a], Jie Cheng[a], Mengmeng Hong[a], Meng Tang[b,c,*], Fashui Hong[a,**]

[a] Medical College, Soochow University, Suzhou 215123, China
[b] Key Laboratory of Environmental Medicine and Engineering, Ministry of Education, School of Public Health, Southeast University, Nanjing 210009, China
[c] Jiangsu Key Laboratory for Biomaterials and Devices, Southeast University, Nanjing 210009, China

ARTICLE INFO

Article history:
Received 23 January 2011
Received in revised form 2 April 2011
Accepted 4 April 2011
Available online 22 April 2011

Keywords:
Titanium dioxide nanoparticles
Mice
Hippocampus
Apoptotic pathway

ABSTRACT

Previous studies demonstrate that the exposure to titanium dioxide nanoparticles (TiO_2 NPs) damages the central nervous system of mice; however, very little is known about the effects of TiO_2 NPs on hippocampal apoptosis or its molecular mechanism. The present study investigated the molecular mechanism associated with hippocampal apoptosis in mice induced by intragastric administration of TiO_2 NPs for consecutive 60 days. Our findings indicate that TiO_2 NPs accumulate in the mouse hippocampus, and this accumulation, in turn, led to hippocampal apoptosis and impairment in spatial recognition memory in mice. In addition, TiO_2 NPs significantly activated caspase-3 and -9, inhibited Bcl-2, and promoted the levels of Bax and cytochrome c. Furthermore, TiO_2 NPs induced accumulation of reactive oxygen species in the mouse hippocampus. These findings suggest that TiO_2 NP-induced apoptosis in the mouse hippocampus may result from an intrinsic pathway, and workers and consumers should take great caution when handling nanomaterials.

1. Introduction

Titanium dioxide nanoparticles (TiO_2 NPs) are widely used in water and air decontamination and as a coloring material in the cosmetics, pharmaceutical and paint industries. However, the impact of these nanoparticles on organisms is not fully understood. Therefore, the primary task of the present study was to clarify the information about safety and potential hazards of products derived from nanomaterials to human health. In recent years, studies have unequivocally showed that TiO_2 NPs accumulate in the liver, kidneys, spleen, lungs, and heart of animals [1,2]. Importantly, previous studies demonstrate that the administration of TiO_2 NPs damage brain neurocyte *in vitro* [3,4], and the nanoparticles are translocated into the central nervous system (CNS) via the olfactory pathway and brain tissue *in vivo* [1,2,5–9]. For example, these studies found that TiO_2 NPs promoted reactive oxygen species (ROS) production, interfered with mitochondrial energy production, and damaged dopaminergic function in brain microglia *in vitro* [3,4]. Furthermore, Wang et al. indicated that TiO_2 NPs were translocated to the olfactory bulb through the olfactory nerve system following inhalation or intranasal instillation, and caused the development of brain lesions in mice, including vacuoles of neurons and fatty degeneration, scattered Nissl bodies, enlarged cell somata and an irregular appearance of neurons in the CA1 region of hippocampus as well as higher inflammation responses [1,5,9]. TiO_2 NPs have been shown to not only increase the lipid peroxidation and protein oxidation in exposed mice, but also induce the release of other specific neurochemicals [6]. For instance, studies have found that TiO_2 NPs were accumulated in the damaged brain of hairless mice after subchronic dermal exposure [10], and promoted neuroinflammatory responses by enhancing microglial activation in the pre-inflamed brain of mice [11]. Furthermore, TiO_2 NPs have been shown to induce apoptosis and oxidative stress in microglia, neurons [3–5,12,13], and Purkinje cells *in vitro* [14]. Our previous studies indicated that TiO_2 NPs exposure was associated with an oxidative injury of the mouse brain [7], and impaired the spatial recognition memory ability of mice [8]. Therefore, these studies confirmed that TiO_2 NPs could enter the CNS, resulting in oxidative stress, inflammatory responses and spatial recognition impairment.

The hippocampus provides a main target of TiO_2 NPs, and hippocampal cells are highly sensitive to ROS following exposure

* Corresponding author at: Key Laboratory of Environmental Medicine and Engineering, Ministry of Education, School of Public Health, Southeast University, Nanjing 210009, China.
** Corresponding author.
E-mail addresses: tm@seu.edu.cn (M. Tang), Hongfsh_cn@sina.com (F. Hong).
[1] These authors contributed equally to this work.

0304-3894/$ – see front matter © 2011 Elsevier B.V. All rights reserved.
doi:10.1016/j.jhazmat.2011.04.027

to nanoparticles [15]. Hippocampus, a major component of the brains of humans and other mammals, belongs to the limbic system, and plays an important role in long-term memory and spatial navigation. We hypothesized that ROS accumulation and memory impairment caused by TiO_2 NPs would be associated with hippocampal apoptosis in mice. To date, studies in this area are limited. Therefore, we conducted an experiment to explore whether developmental TiO_2 NPs exposure would cause hippocampal apoptosis in mice, and we assayed apoptotic cytokine expression in the mouse hippocampus. The primary purpose of our findings was to benefit the understanding of TiO_2 NP-induced effects in brain, and thereby, to arouse the attention of the effects of TiO_2 NPs exposure.

2. Materials and methods

2.1. Chemicals, preparation and characterization

Nanoparticulate anatase TiO_2 was prepared via controlled hydrolysis of titanium tetrabutoxide. The details of the synthesis TiO_2 NP were previously described [16]. Briefly, colloidal titanium dioxide was prepared via a controlled hydrolysis of titanium tetrabutoxide. In a typical experiment, 1 mL of Ti $(OC_4H_9)_4$ was dissolved in 20 mL of anhydrous isopropanol, and was added dropwise to 50 mL of double-distilled water that was adjusted to pH 1.5 with nitric acid under vigorous stirring at room temperature. The temperature of the solution was then raised to 60 °C, and maintained for 6 h to promote better crystallization of nanoparticulate TiO_2 particles. Using a rotary evaporator, the resulting translucent colloidal suspension was evaporated yielding a nanocrystalline powder. The obtained powder was washed three times with isopropanol, and then dried at 50 °C until the evaporation of the solvent was complete. A 0.5% (w/v) hydroxypropylmethylcellulose K4 M (HPMC, K4M) was used as a suspending agent. TiO_2 powder was dispersed onto the surface of 0.5% (w/v) HPMC solution, and then the suspending solutions containing TiO_2 particles were treated ultrasonically for 15–20 min and mechanically vibrated for 2 min or 3 min.

The particle sizes of both the powder and nanoparticle suspended in 0.5% (w/v) HPMC solution after incubation for 12 h and 24 h (5 mg/mL) were determined using a TecnaiG220 transmission electron microscope (TEM) (FEI Co., USA) operating at 100 kV, respectively. In brief, particles were deposited in suspension onto carbon film TEM grids, and allowed to dry in air. Mean particle size was determined by measuring more than 100 individual particles that were randomly sampled. X-ray-diffraction (XRD) patterns were obtained at room temperature with a MERCURY CCD diffractometer (MERCURY CCD Co., Japan) using Ni-filtered Cu Kα radiation. The surface area of each sample was determined by Brunauer–Emmett–Teller (BET) adsorption measurements on a Micromeritics ASAP 2020M+ C instrument (Micromeritics Co., USA). The average aggregate or agglomerate size of the TiO_2 NPs after incubation in 0.5% (w/v) HPMC solution for 12 h and 24 h (5 mg/mL) was measured by dynamic light scattering (DLS) using a Zeta PALS + BI-90 Plus (Brookhaven Instruments Corp., USA) at a wavelength of 659 nm. The scattering angle was fixed at 90°. The Ti^{4+} ions leakage from TiO_2 NPs at time 0 and/or after 12, 24, 48 h of incubation in 0.5% (w/v) HPMC was measured by inductively coupled plasma-mass spectrometry (ICP-MS, Thermo Elemental X7, Thermo Electron Co., Finland) after sample centrifugation and filtration. 20 ng/mL of indium was chosen as an internal standard element, and the detection limit of titanium was 0.074 ng/mL.

2.2. Animals and treatment

It has been previously demonstrated by Wang et al. that sensitivity to TiO_2 exposure was higher in CD-1 (ICR) female mice than CD-1 (ICR) male mice [1]. Therefore, CD-1 (ICR) female mice were used in this study. 80 CD-1 (ICR) female mice (24 ± 2 g) were purchased from the Animal Center of Soochow University (China). All mice were housed in stainless steel cages in a ventilated animal room. Room temperature of the housing facility was maintained at 24 ± 2 °C with a relative humidity of 60 ± 10% and a 12-h light/dark cycle. Distilled water and sterilized food were available for mice *ad libitum*. Prior to dosing, the mice were acclimated to this environment for 5 days. All animals were handled in accordance with the guidelines and protocols approved by the Care and Use of Animals Committee of Soochow University (China). All procedures used in animal experiments conformed to the U.S. National Institutes of Health Guide for the Care and Use of Laboratory Animals [17].

For the experiment, the mice were randomly divided into four groups (N = 20), including a control group (treated with 0.5% (w/v) HPMC) and three experimental groups (5, 10, and 50 mg/kg BW TiO_2 NPs). The mice were weighed, and the TiO_2 NP suspensions were administered to the mice by an intragastric administration every day for 60 days. Any symptoms or mortality were observed and recorded carefully everyday during the 60 days. In addition, the mice were regularly handled and weighed before the behavioral experiments.

2.3. Behavioral apparatus and method

Following the 60 days of TiO_2 NP administration, the acquisition of spatial recognition memory was determined using the Y-maze in mice (N = 20). To assess spatial recognition memory, the Y-maze test consisted of two trials separated by an inter-trial interval (ITI). During the first trial (10-min duration), the mouse was allowed to freely explore only two arms (start arm and other arm) of the maze, and the third arm (novel arm) of the Y-maze was blocked. After a 1 h ITI, the second trial (retention) was conducted where all three arms were accessible, and novelty vs. familiarity was analyzed by comparing the behavior in all three arms. For the second trial, the mouse was placed back in the maze in the same starting arm with free access to all three arms for 5 min. Using a ceiling-mounted CCD camera, all trials were recorded on a VCR. The video recordings were later analyzed to determine the number of entries and time spent in each arm. Data were also expressed as percentage of total time, and the distance spent in the arms was measured every 30 s and during the total 5 min [18]. On the second trial, we also assessed which of the arms was entered first as another reflection of recognizing the novel arm as a measure of discrimination memory [18]. Because retention in the Y-maze test does not last longer than a few hours, this task can be assessed several times in the same animal [19]. Therefore, all mice were tested in the Y-maze three times using 1 h ITI.

2.4. Coefficients of brain and preparation of hippocampus

After behavioral testing using the Y-maze, all mice were first weighed, and then sacrificed after being anesthetized using ether. The brains were quickly removed and placed on ice, and the hippocampi were dissected and frozen at −80 °C.

2.5. Titanium content analysis

Hippocampi were removed from the −80 °C and then thawed, and roughly 0.1 g of the hippocampus was weighed, digested and analyzed for titanium content. Inductively coupled plasma-mass spectrometry (ICP-MS, Thermo Elemental X7, Thermo Electron Co.) was used to analyze the titanium concentration in the samples. For the analysis, an indium concentration of 20 ng/mL was utilized as an internal standard element, and the detection limit of titanium

was 0.074 ng/mL. The data were expressed as nanograms per gram fresh tissue.

2.6. Observation of hippocampal ultrastructure by TEM

Hippocampus was fixed by 2.5% glutaraldehyde in 0.1 mol/dm^3 cacodylate buffer for 2 h, and the samples were washed three times with 0.1 mol dm cacodylate buffer (pH 7.2–7.4) and post-fixed for 1 h in 1% osmium tetraoxide. The specimens were dehydrated by a graded series of ethanol (75, 85, 95, and 100%), and embedded in Epon 812. Ultrathin sections were obtained, contrasted with uranyl acetate and lead citrate, and the sections were visualized using a JEOL 1010 transmission electron microscope (TEM). Hippocampal apoptosis was determined based on the changes in nuclear morphology (e.g., chromatin condensation and fragmentation).

2.7. Analysis of integrity of the hippocampal DNA

DNA was extracted from the mouse hippocampi and purified as described by the manufacturer (Takara company), and A260/A280 (>1.8) indicated that the DNA sample was sufficiently free of protein. The purified DNA was resuspended in Tris–HCl buffer (pH 7.2), and then was stored at 4 °C. The integrity of the hippocampal DNA from various treatments was further examined utilizing agarose gel electrophoresis.

2.8. Expression assay of apoptosis cytokines

The level of mRNA expression of apoptosis-related cytokines (i.e., caspase-3, caspase-8, caspase-9, Bax, Bcl-2, and cytochrome c) were determined using real-time quantitative RT polymerase chain reaction (RT-PCR) [20–22]. Synthesized cDNA was used for the real-time PCR by employing primers that were designed using Primer Express Software according to the software guidelines (Table 1). The gene expression analysis and experimental system evaluation were performed according to the standard curve and quantitation reports. To determine caspase-3, caspase-8, caspase-9, Bax, Bcl-2, and cytochrome c levels in the mouse hippocampus, an enzyme linked immunosorbent assay (ELISA) was performed using commercial kits that are selective for each respective protein (R&D Systems, USA). Manufacturer's instruction was followed. The absorbance was measured on a microplate reader at 450 nm (Varioskan Flash, Thermo Electron, Finland), and the concentration of caspase-3, caspase-8, caspase-9, Bax, Bcl-2, and cytochrome c was calculated from a standard curve for each sample.

2.9. Biochemical parameter assay

Superoxide ion ($O_2^{\bullet-}$) in the mouse hippocampal tissues was measured by determining the reduction of 3′-{1-[(phenylamino) carbonyl]-3,4-tetrazolium}-bis (4-methoxy-6-nitro) benzenesulfonic acid hydrate (XTT) in the presence of $O_2^{\bullet-}$, as described previously by Oliveira et al. [23]. The detection of hydroperoxide (H_2O_2) contents in the hippocampal tissues was carried out by the xylenol orange assay [24].

The activity of superoxide dismutase (SOD) in the hippocampal tissues was assayed by monitoring its ability to inhibit the photochemical reduction of nitroblue tetrazolium (NBT), and monitoring the increase in absorbance at 560 nm followed the production of blue formazan [25]. The activity of catalase (CAT) was measured by analyzing the decrease in the H_2O_2 concentration for 15 s, and then reading the absorbance at 240 nm on a UV-3010 absorption spectrophotometer according to Claiborne [26].

The activity of peroxidase (APx) was assayed using the method described by Reuveni et al. [27]. In addition, the activity of glutathione peroxidase (GSH-Px) was determined by a modified coupled assay procedure of Paglia and Valentine [28]. In order to determine reduced glutathione (GSH) and oxidized glutathione (GSSG) levels, the hippocampi were homogenized as previously described. However, the supernatants were not diluted five-fold as described in the antioxidant enzyme assays. GSH and GSSG contents were estimated using the method described by Hissin and Hilf [29]. Ascorbic acid (AsA) and dehydroascorbic acid (DAsA) determination was also determined using the method described by Jacques-Silva et al. [30]. The content of protein was determined following the Lowry et al. [31] method. Each parameter was determined in five animals.

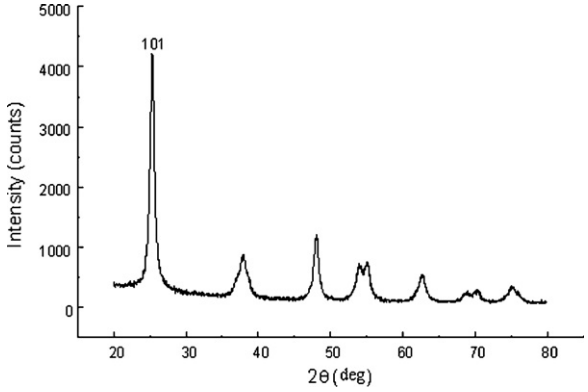

Fig. 1. The (1 0 1) X-ray diffraction peak of anatase TiO_2 NPs. The average grain size was about 5 nm by calculation of Scherrer's equation.

3. Statistical analysis

Statistical analyses were conducted using SPSS 11.7 software. Data were expressed as means ± standard deviation (SD). One-way analysis of variance (ANOVA) was carried out to compare the differences of means among multi-group data. Dunnett's test was performed when each dataset was compared with the solvent-control data. Statistical significance for all tests was judged at a probability level of 0.05 ($p < 0.05$).

4. Results

4.1. TiO_2 NPs characteristics

X-ray diffraction measurements (Fig. 1) show that TiO_2 NPs exhibit the anatase structure, and the average grain size calculated from the broadening of the (1 0 1) XRD peak of anatase was roughly 6.5 nm using Scherrer's equation. The transmission electron micrographs demonstrated that the average particle sizes of powder (Fig. 2a) suspended in HPMC solvent after 12 h and 24 h incubation ranged from 6 to 7 nm, respectively (Fig. 2b and c), which is consistent with the XRD results. The value of the sample surface area was generally smaller than the one estimated from the particle size, and it would seem that the aggregation of the particles may cause such a decline (Table 2). After the 12 h and 24 h incubation, the mean hydrodynamic diameter of TiO_2 NPs in HPMC solvent ranged between 208 and 330 nm (mostly being 294 nm), as measured by DLS (Fig. 3a and b), which indicates that the majority of TiO_2 NPs were clustered and aggregated in solution. In addition, the zeta potential was 7.57 mV and 9.28 mV, respectively, and the particle characteristics for the TiO_2 NPs used in this study are summarized in Table 2. The leakage of Ti^{4+} ions from 12 h, 24 h and 48 h incubation of TiO_2 NPs in HPMC after centrifugation was measured by ICP-MS. However, Ti^{4+} contents were not detected in filtrate, which are higher than the detection limit of 0.074 ng/mL

Table 1
Real time PCR primer pairs. PCR primers used in the gene expression analysis.

Gene name	Description	Primer sequence	Primer size (bp)
Refer-actin	mactin f mactin r	GAGACCTTCAACACCCCAGC ATGTCACGCACGATTTCCC	263
Caspase-8	mcaspase-8 F mcaspase-8 R	ATCTGCTGTATCCCAGC AGGCACTCCTTTCTGGAAGTTAC	180
Caspase-9	mcaspase-9 F mcaspase-9 R	GCGGTGGTGAGCAGAAAGA CCTGGGAAGGTGG AGTAGGA	190
Caspase-3	mcaspase-3 F mcaspase-3 R	CTGACTGGAAAGCCGAAACTC GACTGGATGAACCACGACCC	203
Bax	mbax F mbax R	GGATGCGTCCACCAAGAAG CAAAGTAGAAGAGGGCAACCAC	194
Bcl-2	mbcl-2F mbcl-2 R	TGTGGTCCATCTGACCCTCC ACATCTCCCTGTTGACGCTCT	224
Cytochrome c	mcytochrome c F mcytochrome c R	CATCCCTTGACATCGTGCTT GGGTAGTCTGAGTAGCGTCGTG	250

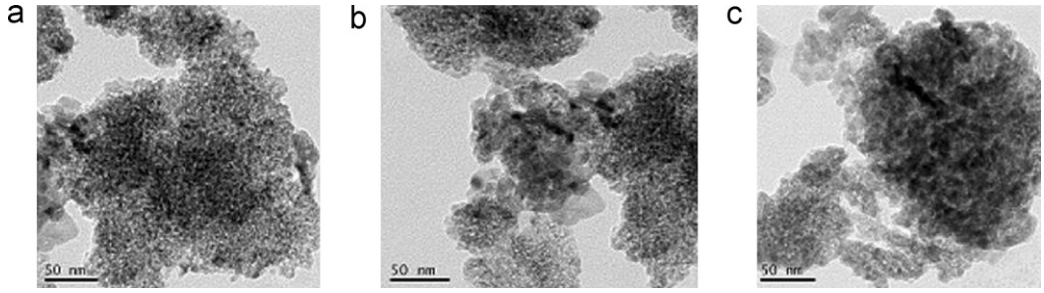

Fig. 2. Transmission electron microscope (TEM) image of anatase TiO_2 NPs particles. (a) TiO_2 NPs powder; (b) TiO_2 NPs suspended in HPMC solvent after incubation for 12 h; (c) TiO_2 NPs suspended in HPMC solvent after incubation for 24 h. TEM images showed that the sizes of the TiO_2 NPs powder or suspended in HPMC solvent for 12 h, 24 h were distributed from 5 to 6 nm, respectively.

Table 2
characteristics of TiO_2 NPs.

Sample	Crystallite size (nm)	Phase	Surface area (m^2/g)	Composition	Zeta potential (mV)
TiO_2NPs	6.5	Anatase	174.8	Ti, O	7.57[a], 9.28[b]

[a] Zeta potential after the 12 h incubation in HPMC solvent.
[b] Zeta potential after the 24 h incubation in 0.5% (w/v) HPMC solvent.

(not listed). Therefore, these results suggested that the Ti^{4+} ions leakage from TiO_2 NPs.

4.2. Titanium content

The contents of titanium in the mouse hippocampus are shown in Fig. 4. With increasing intragastric doses of TiO_2 NPs, the titanium accumulation in the mouse hippocampus was significantly elevated ($p < 0.01$). This accumulation of titanium in hippocampus may damage the mouse hippocampus and impair spatial recognition memory in mice, which is confirmed by the further observation of mouse hippocampal neuron ultrastructure and the behavioral assay of memory in mice.

4.3. Hippocampal neuron ultrastructure evaluation

The changes of neuron ultrastructure in the mouse hippocampus are presented in Fig. 5. It was observed that the mouse neuron in the control group and in the 5 mg/kg BW TiO_2 NPs-treated group contained round nuclei with homogeneous chromatin (Fig. 5a and b), consistent with a normal neuron. However, the ultrastructure of the neuron from the 10 mg/kg BW TiO_2 NPs-treated group presented significant shrinkage of the nucleus (Fig. 5c), and hippocampal neurons treated with 50 mg/kg BW TiO_2 NPs indicated a significant shrinkage of the nuclear membrane as well as chromatin marginalization (Fig. 5d). These phenotypes represent classical morphological characteristics of apoptosis. Thus, the results suggested that TiO_2 NP exposure caused neuron apoptosis in the mouse hippocampus, which may affect spatial recognition memory in mice.

4.4. Assay of DNA ladder from hippocampi

In order to further confirm whether TiO_2 NP exposure is associated with apoptosis in the mouse hippocampus, we performed gel electrophoresis (Fig. 6). Both the control and 5 mg/kg BW TiO_2 NP-treated group showed single stranded DNA. However, hippocampal DNA from 10 and 50 mg/kg BW TiO_2 NP-treated groups generated a classical ladder; therefore, the higher doses of TiO_2 NPs could cause hippocampal apoptosis in mice, which would be consistent with the TEM observation.

4.5. Apoptotic cytokines expression

Both the neuron ultrastructure observations and DNA ladder assay indicate that apoptosis is occurring in the mouse hippocampal neurons. To confirm the role of the apoptosis-induced signaling pathway in the TiO_2 NP-induced hippocampal

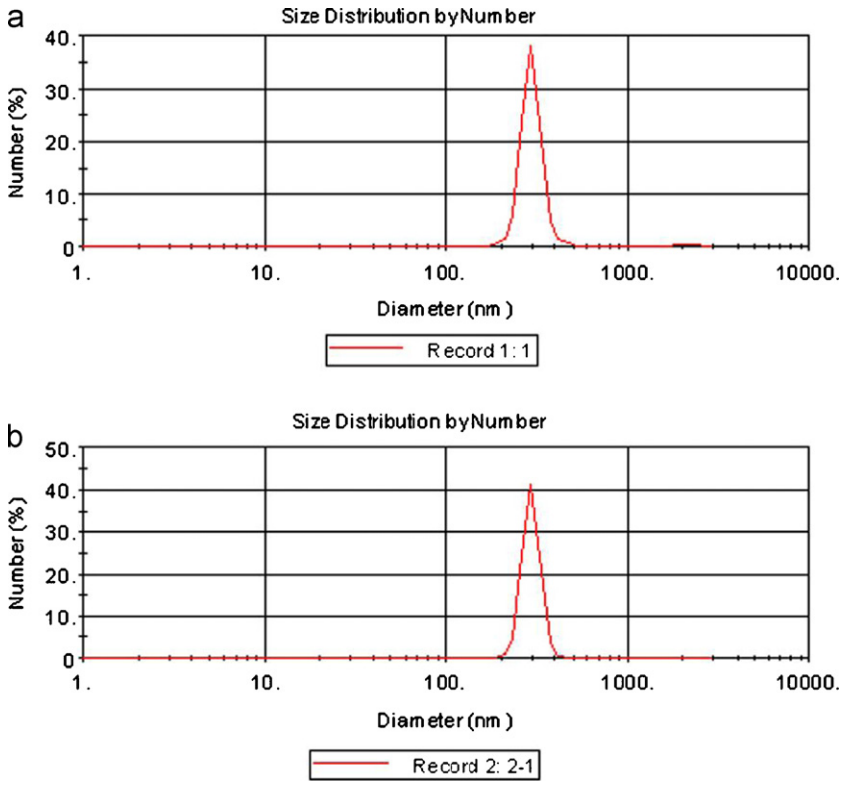

Fig. 3. Hydrodynamic diameter distribution of TiO_2 NPs in HPMC solvent using DLS characterization. (a) Incubation for 12 h; (b) incubation for 24 h.

Table 3
Effect of TiO_2 NPs on the amplification of apoptosis factor mRNA of the mouse hippocampus by real-time PCR analysis after intragastric administration with TiO_2 NPs for consecutive 60 days.

Ratio of gene/actin	TiO_2 NPs (mg/kg BW)			
	0	5	10	50
Caspase-8/actin	0.062 ± 0.003a	0.061 ± 0.003a	0.064 ± 0.003a	0.060 ± 0.003a
Caspase-9/actin	0.010 ± 0.000a	0.016 ± 0.001b	0.029 ± 0.001c	0.046 ± 0.002d
Caspase-3/actin	0.033 ± 0.002a	0.039 ± 0.002a	0.110 ± 0.006b	0.210 ± 0.011c
Bax/actin	0.006 ± 0.000a	0.007 ± 0.000a	0.012 ± 0.001b	0.040 ± 0.002c
Bcl-2/actin	0.097 ± 0.005a	0.070 ± 0.004b	0.043 ± 0.002c	0.021 ± 0.001d
Cytochrome c/actin	13.006 ± 0.650a	16.766 ± 0.838b	18.831 ± 0.942c	56 001 ± 2.800d

Treatments with different letters indicate significantly different values ($p < 0.05$). Values represent means ± SD, $N = 5$.

Table 4
Effect of TiO_2 NPs on the apoptosis protein level of the mouse hippocampus by ELISA analysis after intragastric administration with TiO_2 NPs for consecutive 60 days.

Protein expression	TiO_2 NPs (mg/kg BW)			
	0	5	10	50
Caspase-8 (pg/mg tissue)	8.71 ± 0.44a	8.64 ± 0.43a	8.91 ± 0.44a	8.88 ± 0.44a
Caspase-9 (pg/mg tissue)	84.47 ± 4.22a	102.89 ± 5.14b	114.98 ± 5.75c	120.67 ± 6.03c
Caspase-3 (pg/mg tissue)	35.61 ± l.78a	42.73 ± 2.14b	52.35 ± 2.62b	89.57 ± 4.48c
Bax (ng/mg tissue)	77.19 ± 3.86a	96.82 ± 4.84b	120.46 ± 6.02c	206.96 ± 10.35c
Bcl-2 (ng/mg tissue)	29.89 ± 1.49a	25.71 ± 1.29b	24.55 ± 1.23b	18.41 ± 0.92c
Cytochrome c (pg/mg tissue)	86.36 ± 4.32a	123.06 ± 6.15b	135.44 ± 6.77c	146.77 ± 7.34d

Treatments with different letters indicate significantly different values ($p < 0.05$). Values represent means ± SD, $N = 5$.

apoptosis, real-time quantitative RT-PCR and ELISA were used to detect alterations of the apoptosis-related genes and their proteins levels in the TiO_2 NP-treated mice (Tables 3 and 4). Tables 3 and 4 indicate that TiO_2 NP exposure did not significantly change the levels of caspase-8 expression ($p > 0.05$); however, TiO_2 NP exposure did significantly induce caspase-9 and caspase-3 expression in the treated mouse hippocampus ($p < 0.05$ or 0.01). Tables 2 and 3 also indicate that TiO_2 NP exposure significantly suppressed Bcl-2 gene and protein expression, but promoted the expression of Bax and cytochrome c in the hippocampus compared with the control ($p < 0.05$ or 0.01).

4.6. ROS production and lipid peroxidation

Fig. 7 shows how exposure to TiO_2 NPs changes the production rate of O_2^- and H_2O_2 in the mouse hippocampus. TiO_2 NP exposure caused a dramatic increase of the generating rate of ROS in hippocampus in mice ($p < 0.05$ or 0.01).

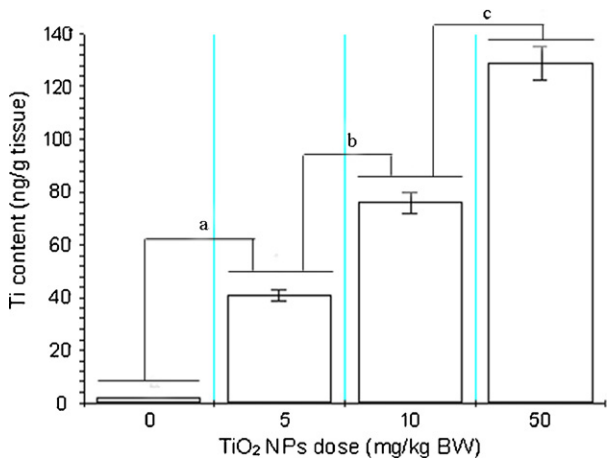

Fig. 4. The contents of titanium in hippocampus of ICR female mice after intragastric administration with TiO_2 NPs for 60 days. Treatments with different letters indicate significantly different values ($p < 0.05$). Values represent means ± SD, $N = 5$.

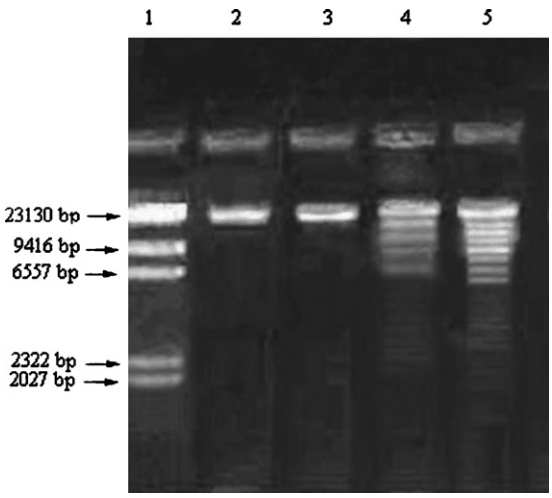

Fig. 6. Assay of DNA ladder from hippocampi of mice caused by intragastric administration with TiO_2 NPs for consecutive 60 days. (1) DNA marker; (2) control exhibits single strand DNA; (3) 5 mg/kg BW TiO_2 NPs exhibits single strand DNA; (4) 10 mg/kg TiO_2 NP exhibits DNA ladder; (5) 50 mg/kg BW TiO_2 NPs exhibits DNA ladder.

4.7. Antioxidant capacity

Figs. 8 and 9 demonstrate the activities of enzymatic and non-enzymatic antioxidants in the mouse hippocampus caused by TiO_2 NP exposure. With increasing intragastric doses of TiO_2 NPs, the activities of SOD, CAT, APx and GSH-Px showed significant decreases, and the ratios of AsA to DAsA and GSH to GSSGG in hippocampus also showed a significant reduction ($p < 0.05$ or 0.01). These findings suggest that TiO_2 NP exposure decreased the antioxidant capacity of the mouse hippocampus.

4.8. Evaluation of spatial recognition memory

Fig. 10 presents the effects of TiO_2 NP exposure on the spatial recognition memory in mice. The percentage of duration to explore the novel arm was significantly higher than the start and other arms for the unexposed mice ($p < 0.01$), and the percentage of duration to explore the novel arm was significantly higher than the start and

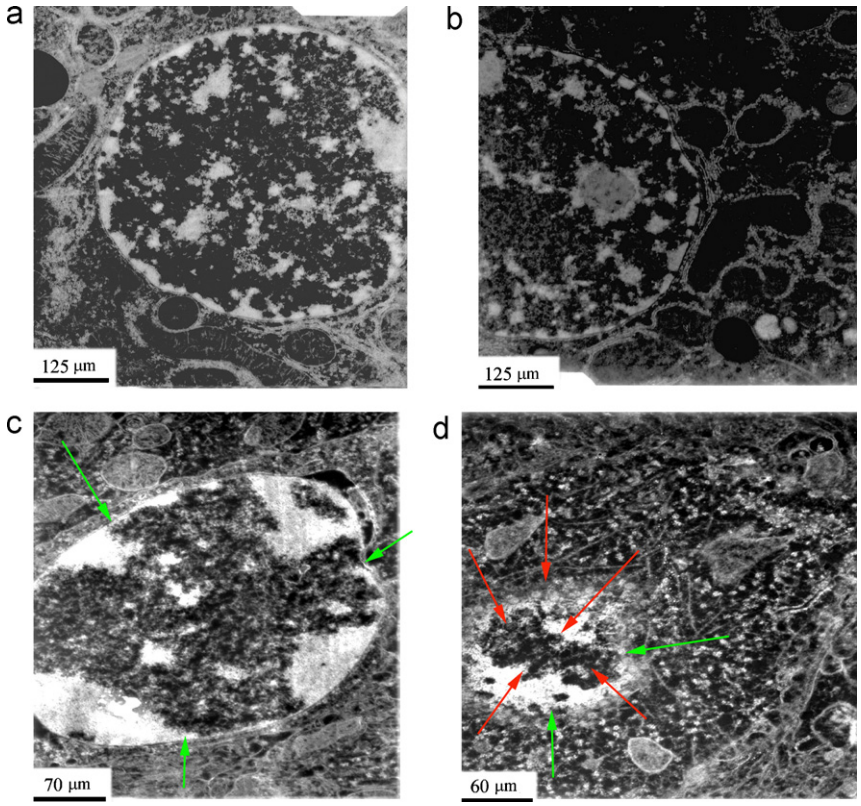

Fig. 5. Ultrastructure of hippocampal neuron in female mice caused by intragastric administration with TiO_2 NPs for consecutive 60 days. (a) Control: chromatin is nucleus with homogeneous chromatin, and nucleolus is attached to nuclear membrane side in the hippocampus CA neuron; (b) 5 mg/kg BW TiO_2 NPs: chromatin exhibits nucleus with homogeneous chromatin in the hippocampus CA neuron; (c) 10 mg/kg BW TiO_2 NPs exhibits shrinkage of nucleus in the hippocampus CA neuron (green arrows) compared with control and 5 mg/kg BW TiO_2 NPs, respectively; (d) 50 mg/kg BW TiO_2 NPs suggests significant shrinkage of nuclear membrane (green arrows)and chromatin marginalization ((red arrows)) in the hippocampus CA neuron compared with control, 5, and 10 mg/kg BW TiO_2 NPs, respectively. (For interpretation of the references to color in this figure legend, the reader is referred to the web version of the article.)

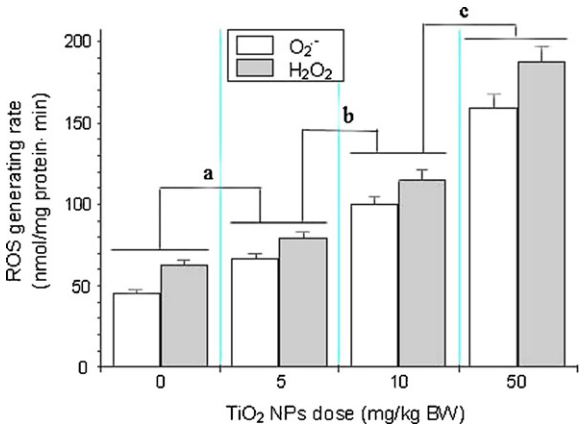

Fig. 7. The ROS generating rate of hippocampus of ICR mice after intragastric administration with TiO_2 NPs for consecutive 60 days. Treatments with different letters indicate significantly different values ($p < 0.05$). Values represent means ± SD, $N = 5$.

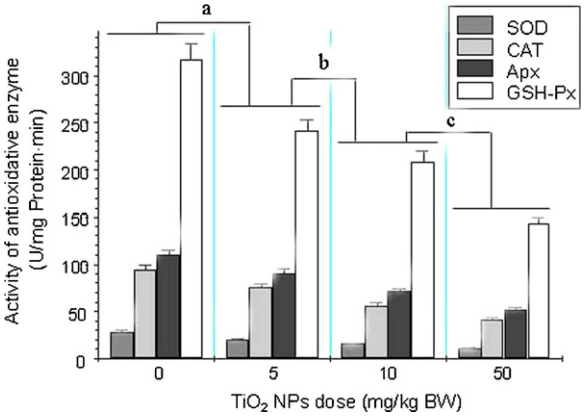

Fig. 8. The activities of antioxidative enzymes of hippocampus of ICR mice after intragastric administration with TiO_2 NPs for consecutive 60 days. Treatments with different letters indicate significantly different values ($p < 0.05$). Values represent means ± SE, $N = 5$.

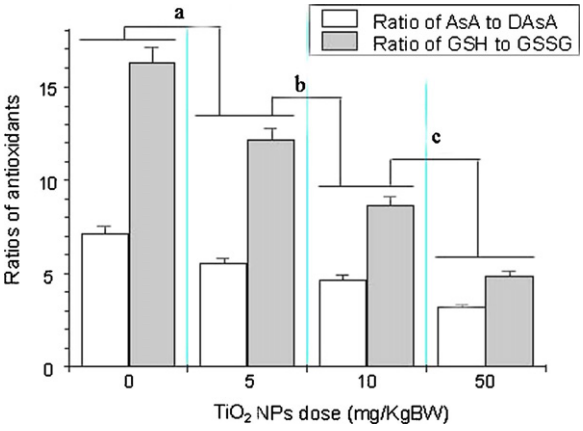

Fig. 9. The ratios of AsA to DAsA and GSH to GSSGG of the mouse hippocampus after intragastric administration with TiO_2 NPs for consecutive 60 days. Treatments with different letters indicate significantly different values ($p < 0.05$). Values represent means ± SD, $N = 5$.

other arms for the 5 mg/kg BW TiO_2 NP mice ($p < 0.05$), respectively. However, the percentage of duration for 10 and 50 mg/kg BW TiO_2 NPs mice to explore the novel arm was not statistically significant different from the start arm, and lower than the duration in the other arm ($p > 0.05$). These findings suggest that higher doses of TiO_2 NP exposure impair the spatial recognition memory in mice.

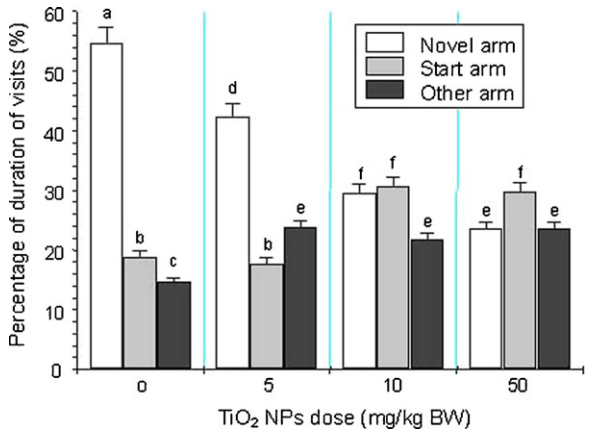

Fig. 10. Effect of TiO_2 NPs on the spatial recognition memory of mice in Y-maze after intragastric administration with TiO_2 NPs for the consecutive 60 days. Treatments with different letters indicate significantly different values ($p < 0.05$). Values represent means ± SD, $N = 20$.

5. Discussion

To understand the underlying mechanism for the brain injury of mice caused by exposure to TiO_2 NPs, the present study was designed to investigate the relevant apoptosis pathways in the mouse hippocampus. Our data indicate that titanium was significantly accumulated in the mouse hippocampus (Fig. 4), and indicate that TiO_2 NPs can easily cross the blood–brain barrier (BBB) into the hippocampus, depositing TiO_2 NPs in the CNS and damaging the barrier integrity [32–34]. Apoptosis is characterized by cellular and nuclear shrinkage and condensation followed by DNA ladder, nuclear fragmentation, cellular budding, and the formation of apoptotic bodies [35]. Due to TiO_2 NP deposition, we observed nuclear shrinkage and chromatin condensation in the nucleus of neurons (Fig. 5) and the DNA ladder in the mouse hippocampus (Fig. 6), which are classical characteristics of apoptosis caused by TiO_2 NPs. Previous studies demonstrate that TiO_2 NP exposure can induce apoptosis or necrosis in different types of cells or organs, such as microglia, neurons [3–5,12,13], Purkinje cells [14], mesenchymal stem cells [36], fibroblasts [37], lymphoblastoid cells [38], human bronchial epithelial cells [39], BEAS-2B cells [40], spleen [41], and liver [42].

Apoptosis can be triggered through two principal signaling pathways: (1) the death receptor-mediated extrinsic apoptotic pathway and (2) the recruitment of adaptor proteins followed by the activation of caspase-8 and the mitochondrion-mediated intrinsic apoptotic pathway. The hippocampal apoptotic processes may hypothetically occur via the mitochondrion-mediated pathway. In this pathway mitochondrial permeability is first increased, and then followed by the release of apoptogenic factors such as cytochrome c and the activation of initiator caspase-9 and effector caspase-3 of apoptosis-inducing factor. In addition, the Bcl-2 family proteins are considered as critical regulators of mitochondria-mediated apoptosis by regulating either promoters (e.g., Bax and Bid) or inhibitors (e.g., Bcl-2) of the cell death process [43–45]. In the present study, we observed increases in caspase-3 gene and protein expression associated with hippocampal apoptosis in mice in response to TiO_2 NP exposure, and this response occurred in a dose-dependent manner. Moreover, TiO_2 NPs exposure also significantly increased the gene and protein expression of caspase-9, Bax, and cytochrome c, and significantly suppressed bcl-2 expression in hippocampus of mice (Tables 3 and 4). These findings indicate that TiO_2 NP-induced apoptosis in the mouse hippocampus may be mediated via mitochondrial or the intrinsic pathway.

Apoptosis can also be triggered through the extrinsic pathway that involves the activation of caspase-8. The increase of caspase-8 expression can either directly activate caspase-3 leading to cell apoptosis or indirectly activate caspase-3 resulting in the activation of caspase-9 and the mitochondrial pathway. In the present study, our data indicate that TiO_2 NP exposure activates caspase-9, but not the caspase-8 in the mouse hippocampus (Tables 3 and 4) Therefore, these findings indicate that the hippocampal apoptosis caused by TiO_2 NP exposure may not be mediated via the extrinsic pathway.

ROS is at least one of the triggers for intrinsic apoptosis. In order to further confirm the apoptosis pathways in the hippocampus associated with TiO_2 NP exposure, we assayed ROS accumulation and antioxidant capacity. Our data suggest that the ROS levels (such as $O_2^{\bullet -}$, H_2O_2) significantly increased (Fig. 7), while the scavengers of ROS (such as SOD, CAT, APx, GSH-Px, GSH, and AsA) markedly decreased in the hippocampus of TiO_2 NP treated mice (Figs. 8 and 9), consistent with apoptosis. Previous studies demonstrate that the toxicity of nano-sized particles is mediated through the induction of ROS [45–47]. Likewise, ROS increases are closely related to the induction of apoptotic and necrotic cell death in cell cultures [45,48]. TiO_2 NPs could be phagocytized by neurons and microglia, which then release ROS ($^{\bullet}OH$ and $O_2^{\bullet -}$) and cause apoptosis [3–5]. ROS has also been shown to increase the permeability of mitochondrial membrane [49], and cause oxidative damage to DNA [50]. Therefore, the importance of ROS in triggering intrinsic apoptosis in TiO_2 NP-induced apoptosis of the mouse hippocampus is consistent with these findings.

Because the hippocampus plays important roles in long-term memory and spatial navigation, TiO_2 NP exposure that causes hippocampal neuron apoptosis may also result in impairment in the hippocampal function. Therefore, we evaluated the effect of TiO_2 NPs on spatial recognition memory in mice. Utilizing the two-trial Y-maze task, the present article demonstrates significant arm effects on the percentage of total duration and number of visits during the retention test. However, after exposure to TiO_2 NPs, the time spent in the familiar start and other arms for mice were gradually increased, while the time spent in the unfamiliar novel arm was gradually decreased. However, the time spent in the familiar start and other arms was lower than that of the unfamiliar novel arm for unexposed mice (Fig. 10). Dellu et al. [19] clearly demonstrated that the first choice for novel arm can be utilized to test discrimination memory. The previous reports also demonstrate by Y-maze testing that TiO_2 NPs exposure decreased the learning and memory ability of mice [6]. As compared to unexposed mice, this obvious reduction of spatial recognition memory in mice was caused by exposure to TiO_2 NPs, and was associated with hippocampal apoptosis.

In summary, this study demonstrated that apoptosis induced by exposure to TiO_2 NPs in the mouse hippocampus was mediated primarily through the intrinsic apoptosis pathway. In addition, ROS overproduction was among the probable triggers of TiO_2 NP-induced apoptosis in hippocampus.

Acknowledgements

This work was supported by A Project Funded by the Priority Academic Program Development of Jiangsu Higher Education Institutions, the National Natural Science Foundation of China (grant no. 30901218), the Major State Basic Research Development Program of China (973 Program) (grant no. 2006CB705602), National Important Project on Scientific Research of China (grant no. 2011CB933404), National Natural Science Foundation of China (grant No.30671782, 30972504).

References

[1] J.X. Wang, G.Q. Zhou, C.Y. Chen, H.W. Yu, T.C. Wang, Y.M. Ma, G. Jia, Y.X. Gao, B. Li, J. Sun, Y.F. Li, F. Jia, Y.L. Zhao, Z.F. Chai, Acute toxicity and biodistribution of different sized titanium dioxide particles in mice after oral administration, Toxicol. Lett. 168 (2007) 176–185.
[2] H.T. Liu, L.L. Ma, J.F. Zhao, J. Liu, J.Y. Yan, J. Ruan, F.S. Hong, Biochemical toxicity of nano-anatase TiO_2 particles in mice, Biol. Trace Elem. Res. 129 (2009) 170–180.
[3] T.C. Long, N. Saleh, R.D. Tilton, G. Lowry, B. Veronesi, Titanium dioxide (P25) produces reactive oxygen species in immortalized brain microglia (BV2): implications for nanoparticle neurotoxicity, Environ. Sci. Technol. 40 (2006) 4346–4352.
[4] T.C. Long, J. Tajuba, P. Sama, N. Saleh, C. Swartz, J. Parker, S. Hester, G.V. Lowry, B. Veronesi, Nanosize titanium dioxide stimulates reactive oxygen species in brain microglia and damages neurons in vitro, Environ. Health Perspect. 115 (11) (2007) 1631–1637.
[5] J.X. Wang, Y. Liu, F. Jiao, F. Lao, W. Li, Y.Q. Gu, Y.F. Li, C.C. Ge, G.Q. Zhou, B. Li, Y.L. Zhao, Z.F. Chai, C.Y. Chen, Time-dependent translocation and potential impairment on central nervous system by intranasally instilled TiO_2 nanoparticles, Toxicology 254 (2008) 82–90.
[6] J.X. Wang, C.Y. Chen, Y. Liu, F. Jiao, W. Li, F. Lao, Y.F. Li, B. Li, C.C. Ge, G.Q. Zhou, Y.X. Gao, Y.L. Zhao, Z.F. Chai, Potential neurological lesion after nasal instillation of TiO_2 nanoparticles in the anatase, rutile crystal phases, Toxicol. Lett. 183 (2008) 72–80.
[7] L.L. Ma, J. Liu, N. Li., J. Wang, Y.M. Duan, J.Y. Yan, H.T. Liu, H. Wang, F.S. Hong, Oxidative stress in the brain of mice caused by translocated nanoparticulate TiO_2 delivered to the abdominal cavity, Biomaterials 31 (2010) 99–105.
[8] R.P. Hu, X.L. Gong, Y.M. Duan, N. Li, Y. Che, Y.L. Cui, M. Zhou, C. Liu, H. Wang, F.S. Hong, Neurotoxicological effects and the impairment of spatial recognition memory in mice caused by exposure to TiO_2 nanoparticles, Biomaterials 31 (2010) 8043–8050.
[9] J.X. Wang, C.Y. Chen, H.W. Yu, J. Sun, B. Li, Y.F. Li, Y.X. Gao, W. He, Y.Y. Huang, Z.F. Chai, Y.L. Zhao, X.Y. Deng, H.F. Sun, Distribution of TiO_2 particles in the olfactory bulb of mice after nasal inhalation using microbeam SRXRF mapping techniques, J. Radioanal. Nucl. Chem. 272 (3) (2007) 527–531.
[10] J. Wu, W. Liu, C.B. Xue, S.C. Zhou, F.L. Lan, L. Bi, Toxicity and penetration of TiO_2 nanoparticles in hairless mice and porcine skin after subchronic dermal exposure, Toxicol. Lett. 191 (1) (2009) 1–8.
[11] J.A. Shin, E.J. Lee, S.M. Seo, H.S. Kim, J.L. Kang, E.M. Park, Nanosized titanium dioxide enhanced inflammatory responses in the septic brain of mouse, Neuroscience 165 (2010) 445–454.
[12] Y. Yu, W. Ren, B. Ren, Nanosize titanium dioxide cause neuronal apoptosis: a potential linkage between nanoparticle exposure and neural disorder, Neurol. Res. (2008), doi:10.1179/17431 3208X 305391.
[13] X.B. Li, S.Q. Xu, Z.R. Zhang, J.S. Hermann, Apoptosis induced by titanium dioxide nanoparticles in cultured murine microglia N9 cells, Chin. Sci. Bull. 54 (20) (2009) 3830–3836.
[14] K. Takeda, K. Suzuki, A. Ishihara, M. Kubo-Irie, R. Fujimoto, M. Tabata, S. Oshio, Y. Nihei, T. Ihara, M. Sugamata, Nanoparticles transferred from pregnant mice to their offspring can damage the genital and cranial nerve systems, J. Health Sci. 55 (1) (2009) 95–102.
[15] Z. Yang, Z.W. Liu, R.P. Allaker, P. Reip, J. Oxford, Z. Ahmad, G. Ren, A review of nanoparticle functionality and toxicity on the central nervous system, J. R. Soc. Interface 7 (2010) S411–S422.
[16] P. Yang, C. Lu, N. Hua, Y. Du, Titanium dioxide nanoparticles co-doped with Fe^{3+} and Eu^{3+} ions for photocatalysis, Mater. Lett. 57 (2002) 794–801.
[17] National Institutes of Health (NIH), Guide for the Care and Use of Laboratory Animals, National Academy Press, Washington, DC, 1996.
[18] Y. Akwa, N. Ladurelle, D.F. Covey, E.E. Baulieu, The synthetic enantiomer of pregnenolone sulfate is very active on memory in rats and mice, even more so than its physiological neurosteroid counterpart: distinct mechanisms? Proc. Natl. Acad. Sci. U.S.A. 98 (2001) 14033–14037.
[19] F. Dellu, A. Contarino, H. Simon, G.F. Koob, L.H. Gold, Genetic differences in response to novelty and spatial memory using a two-trial recognition task in mice, Neurobiol. Learn. Mem. 73 (2000) 31–48.
[20] K.J. Livak, T.D. Schmittgen, Analysis of relative gene expression data using real-time quantitative PCR and the 2(-Delta Delta C(T)) method, Methods 25 (2001) 402–408.
[21] L.D. Ke, Z.A. Chen, reliability test of standard-based quantitative PCR: exogenous vs endogenous standards, Mol. Cell Probes 14 (2) (2000) 127–135.
[22] W.H. Liu, A. David, Saint validation of a quantitative method for real time PCR kinetics, Biochem. Biophys. Res. Commun. 294 (2002) 347–353.
[23] C.P. Oliveira, F.P. Lopasso, F.R. Laurindo, R.M. Leitao, A.A. Laudanna, Protection against liver ischemia–reperfusion injury in rats by silymarin or verapamil, Transplant. Proc. 33 (2001) 3010–3014.
[24] J. Nourooz-Zadeh, J. Tajaddini-Sarmadi, S.P. Wolff, Measurement of plasma hydroperoxide concentrations by the ferrous oxidation-xylenol orange assay in conjunction with triphenylphosphine, Anal. Biochem. 220 (1994) 403–409.
[25] C. Beauchamp, I. Fridovich, Superoxide dismutase: improved assays and assay applicable to acrylamide gels, Anal. Biochem. 44 (1971) 276–286.
[26] A. Claiborne, Catalase activity, in: R.A. Greenwaid (Ed.), Handbook of Methods for Oxygen Free Radical Research, CRC Press, Boca Raton, FL, 1985.
[27] R. Reuveni, M. Shimoni, Z. Karchi, J. Kuc, Peroxidase activity as a biochemical marker for resistance of muskmelon (*Cucumis melo*) to seudoperno spora cubensis, Phytopathology 82 (1992) 749–753.

[28] D.E. Paglia, W.N. Valentine, Studies on the quantitative and qualitative characterization of erythrocyte glutathione peroxidase, J. Lab. Clin. Med. 70 (1967) 158–169.
[29] P.J. Hissin, R. Hilf, A fluorometric method for determination of oxidized and reduced glutathione in tissues, Anal. Biochem. 74 (1976) 214–226.
[30] M.C. Jacques-Silva, C.W. Nogueira, L.C. Broch, E.M. Flores, J.B.T. Rocha, Diphenyl diselenide and ascorbic changes deposition of selenium and ascorbic in liver and brain of mice, Pharmacol. Toxicol. 88 (2001) 119–125.
[31] O.H. Lowry, N.J. Rosebrough, A.L. Farr, R.J. Randall, Protein measurement with the folin phenol reagent, J. Biol. Chem. 193 (1951) 265–275.
[32] G. Oberdörster, Z. Sharp, V. Atudorei, A. Elder, R. Gelein, W. Kreyling, C. Cox, Translocation of inhaled ultrafine particles to the brain, Inhal. Toxicol. 16 (2004) 437–445.
[33] H.F. Wang, J. Wang, X.Y. Deng, H.F. Shi., Z. Sun, Z.N. Gu., Y.F. Liu, Y.L. Zhao, Biodistribution of carbon single-wall carbon nanotubes in mice, J. Nanosci. Nanotechnol. 4 (2004) 1019–1024.
[34] J.T. Kwon, S.K. Hwang, H. Jin, D.S. Kim, A. Mina-Tehrani, H.J. Yoon, M. Chop, T.J. Yoon, D.Y. Han, Y.W. Kang, B.I. Yoon, J.K. Lee, M.H. Cho, Body distribution of inhaled fluorescent magnetic nanoparticles in the mice, J. Occup. Health 50 (2008) 1–6.
[35] M.L. Wang, R. Tuli, P.A. Manner, P.F. Sharkey, D.J. Hall, R.S. Tuan, Direct and indirect induction of apoptosis in human mesenchymal stem cells in response to titanium particles, J. Orthop. Res. 21 (2003) 697–707.
[36] E. Osano, J. Kishi, Y. Takahashi, Phagocytosis of titanium particles and necrosis in TNF-alpha-resistant mouse sarcoma L929 cells, Toxicol. In Vitro 17 (2003) 41–47.
[37] J.J. Wang, B.J. Sanderson, H. Wang, Cyto- and genotoxicity of ultrafine TiO_2 particles in cultured human lymphoblastoid cells, Mutat. Res. 628 (2007) 99–106.
[38] E.J. Park, J. Yi, K.H. Chung, D.Y. Ryu, J.H. Choi, K. Park, Oxidative stress and apoptosis induced by titanium dioxide nanoparticles in cultured BEAS-2B cells, Toxicol. Lett. 180 (2008) 222–229.
[39] Y.L. Shi, F. Wang, J.B. He, S. Yadav, H. Wang, Titanium dioxide nanoparticles cause apoptosis in BEAS-2B cells through the caspase 8/t-Bid-independent mitochondrial pathway, Toxicol. Lett. 196 (2010) 21–27.
[40] N. Li, Y.M. Duan, M.M. Hong, L. Zheng, M. Fei, X.Y. Zhao, J. Wang, Y.L. Cui, H.T. Liu, J.W. Cai, S.J. Gong, H. Wang, F.S. Hong, Spleen injury and apoptotic pathway in mice caused by titanium dioxide nanoparticles, Toxicol. Lett. 195 (2010) 161–168.
[41] Y.L. Cui, X.L. Gong, R.P. Hu, H.T. Liu, M.M. Hong, M. Zhou, J. Wang, L. Wang, H. Wang, F.S. Hong, Hepatocyte apoptosis and its molecular mechanisms in mice caused by nanoparticulate anatase titanium dioxide, J. Hazard. Mater. 183 (2010) 874–880.
[42] Z. Darzynkiewicz, G. Juan, X. Li, W. Gorczyca, T. Murakami, F. Traganos, Cytometry in cell necrobiology: analysis of apoptosis and accidental cell death (necrosis), Cytometry 27 (1997) 1–20.
[43] A. Suliman, A. Lam, R. Datta, R.K. Srivastava, Intracellular mechanisms of TRAIL: apoptosis through mitochondrial-dependent and -independent pathways, Oncogene 20 (2001) 2122–2133.
[44] K. Kandasamy, S.M. Srinivasula, E.S. Alnemri, C.B. Thompson, S.J. Korsmeyer, J.L. Bryant, R.K. Srivastava, Involvement of proapoptotic molecules Bax and Bak in tumor necrosis factor-related apoptosis-inducing ligand (TRAIL)-induced mitochondrial disruption and apoptosis: differential regulation of cytochrome c and Smac/DIABLO release, Cancer Res. 63 (2003) 1712–1721.
[45] J.C. Yao, Z.Z. Jiang, W.G. Duan, J.F. Huang, L.Y. Zhang, L. Hu, F. Li, Y.J. Xiao, B. Shu, C.H. Liu, Involvement of mitochondrial pathway in triptolide-induced cytotoxicity in human normal liver L-02 cells, Biol. Pharm. Bull. 31 (2008) 592–597.
[46] A. Nel, T. Xia, L. Madler, N. Li, Toxic potential of materials at the nanolevel, Science 311 (5761) (2006) 622–627.
[47] S. Ueda, H. Masutani, H. Nakamura, T. Tanaka, M. Ueno, J. Yodoi, Redox control of cell death, Antioxid. Redox Signal. 4 (3) (2002) 405–414.
[48] M. Ott, V. Gogvadze, S. Orrenius, B. Zhivotovsky, Mitochondria, oxidative stress and cell death, Apoptosis 12 (5) (2007) 913–922.
[49] J Yang, L.J. Wu, S. Tashino, S. Onodera, T. Ikejima, Critical roles of reactive oxygen species in mitochondrial permeability transition in mediating evodiamine-induced human melanoma A375-S2 cell apoptosis, Free Radic. Res. 41 (2007) 1099–1108.
[50] K. Bhattacharya, M. Davoren, J. Boertz, R.P. Schins, E. Hoffmann, E. Dopp, Titanium dioxide nanoparticles induce oxidative stress and DNA-adduct formation but not DNA-breakage in human lung cells, Part. Fibre Toxicol. 6 (2009) 17.